High-resolution laser spectroscopy and photodissociation dynamics of OH+

Peter J Sarre, David J Rodgers, Andrew D Batey

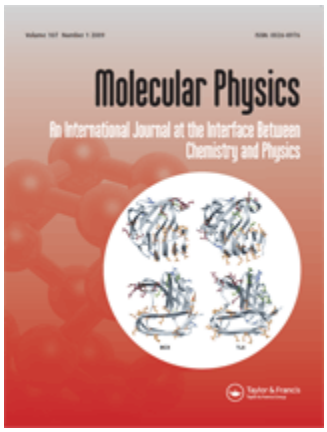

High-resolution laser spectroscopy and photodissociation dynamics of OH^+

Journal:	*Molecular Physics*
Manuscript ID:	TMPH-2006-0062.R1
Manuscript Type:	Full Paper
Date Submitted by the Author:	10-Dec-2006
Complete List of Authors:	Sarre, Peter; The University of Nottingham, Chemistry Rodgers, David; The University of Nottingham, Chemistry Batey, Andrew; The University of Nottingham, Chemistry
Keywords:	Electronic, spectroscopy, dynamics, predissociation

High-resolution laser spectroscopy and photodissociation dynamics of OH^+

D.J. RODGERS[1], A.D. BATEY[2] and P.J. SARRE*

School of Chemistry, The University of Nottingham, University Park, Nottingham, NG7 2RD, UK

* Author for correspondence. e-mail: Peter.Sarre@Nottingham.ac.uk

1. Current address: Faculty of Applied Sciences, University of the West of England, Coldharbour Lane, Bristol, BS16 1QY, UK
2. Current address: Institute of Astronomy, University of Cambridge, Madingley Road, Cambridge. CB3 0HA, UK

Key words. Electronic, spectroscopy, dynamics, predissociation

---

[Telephone 0115 951 3460]
[Fax 0115 951 3562]

Abstract

We report high-resolution spectra of the $c^1\Pi$ - $b^1\Sigma^+$ and $c^1\Pi$ - $a^1\Delta$ electronic transitions of OH^+ obtained by detecting O and O^+ photofragments which arise from predissociation of the $c^1\Pi$ electronic state. Five vibrational bands of the $c^1\Pi$ - $b^1\Sigma^+$ system and three of the $c^1\Pi$ - $a^1\Delta$ system of $^{16}OH^+$ were recorded and molecular parameters derived from the analysis. Spectra of the $^{16}OD^+$ isotopic modification were also taken. A study of perturbations between the $A^3\Pi$ and $b^1\Sigma^+$ states leads to improved determination of the spin-orbit interaction between these states and their relative energies. A selective predissociation mechanism operates with laser excitation to $^1\Pi$ (*e*) levels strongly weighted towards formation of O + H^+, whereas $^1\Pi$ (*f*) levels yield O^+ + H exclusively. The predissociation decay rates are also dependent on the $c^1\Pi$ state vibrational and rotational quantum numbers. The measured linewidths for $v' = 2$ and 3 are in good agreement with both a theoretical approach based on spectroscopic parameters and the results of high-quality *ab-initio* calculations of Yarkony.

1. Introduction

The OH^+ molecule and its fragmentation are important in a very wide range of fields including molecular spectroscopy, dissociation dynamics, ion-atom scattering, electron-ion recombination, van der Waals complex formation, plasma processes and astrophysics. Spectroscopic studies of gas-phase OH^+ comprise a detailed analysis of the $A^3\Pi$ - $X^3\Sigma^-$ electronic band system observed in emission (see [1] and references therein) and of longer wavelength transitions between levels of the $X^3\Sigma^-$ ground state. The $A^3\Pi$ – $X^3\Sigma^-$ electronic transition of $^{16}OH^+$ exhibits perturbations between rotational levels of v = 1 of the $A^3\Pi$ state and v = 0 of the nearby $b^1\Sigma^+$ state. Merer *et al.* [1] carried out a rotational analysis on the triplet system allowing for these perturbations and obtained molecular parameters for the electronic states as well as the first information on the location and some molecular parameters of the $b^1\Sigma^+$ state. In the first spectroscopic fast-ion-beam experiment on OH^+, Helm, Cosby and Huestis [2] studied a few transitions of the $A^3\Pi$ – $X^3\Sigma^-$ system involving quasi-bound rotational levels of the $A^3\Pi$ state by Doppler-tuning the transitions into resonance with the lines of an argon ion laser. Similar studies of near-threshold levels pumped in the $A^3\Pi$ - $X^3\Sigma^-$ transition of radiatively cooled OH^+ in a storage ring have been reported [3]. Transitions between singlet states ($c^1\Pi$ - $b^1\Sigma^+$) using laser photofragment spectroscopy have been accomplished [4] as well as discovery of an *e/f* symmetry-selective dissociation [5].

Several high-resolution experimental techniques have been employed to probe the $X^3\Sigma^-$ electronic ground state. Laser magnetic resonance transitions in the far-infrared region between components of the lowest few rotational levels in $^{16}OH^+$, $^{18}OH^+$ and $^{16}OD^+$ have been reported [6], N = 1 - 0 rotational absorption spectra have been recorded in the sub-mm range [7,8], an infrared spectrum of the fundamental vibration-rotation band has been obtained [9], and studies of transitions between highly vibrationally excited levels have been made [10]. In an experiment similar in concept to that employed here, infrared predissociation spectra of the OH^+ - He and OH^+ - Ne complexes have been obtained with rotational resolution showing that the equilibrium structure of both of these molecules is linear [11].

In the first recording of a rotational spectrum of a molecular ion in a metastable electronic state, Varberg, Evenson and Brown reported the J = 3-2 transition of OH^+ in its $a^1\Delta$ (v = 0) state by far infrared laser magnetic resonance spectroscopy from which rotational and proton hyperfine parameters were obtained [12].

In this paper we first present high-resolution spectroscopic observations of the $c^1\Pi$ - $b^1\Sigma^+$ and $c^1\Pi$ - $a^1\Delta$ transitions, the latter being its first reported detection. Bands of OH^+ and OD^+ were measured and molecular parameters for the $c^1\Pi$, $b^1\Sigma^+$ and $a^1\Delta$ electronic states derived. Perturbations in the $b^1\Sigma^+$ v = 0 level of $^{16}OH^+$ are observed in the spectra and the deperturbation treatment of Merer et al. [1] has been extended with inclusion of the rotational lines of the $c^1\Pi$ - $b^1\Sigma^+$ transition in a single least-squares fit involving four electronic states. This provides information on the relative energies of the triplet and singlet manifolds and on the interaction between the $A^3\Pi$ and $b^1\Sigma^+$ states.

Secondly, the fragmentation dynamics of OH^+ ($c^1\Pi$) are discussed with reference to measured lifetime broadening, inter-state couplings and a symmetry-dependent interaction that determine the relative yields of $O + H^+$ and $O^+ + H$ products. The results are interpreted in terms of direct and indirect dissociation mechanisms and are compared in detail with an *ab-initio* investigation of the states, their couplings and associated dissociation dynamics by Yarkony [13], in which earlier theoretical studies are referenced.

2. Experimental approach

The technique of fast-ion-beam laser photofragment spectroscopy has been reviewed [14,15] and the apparatus employed for these OH^+ measurements has been described in detail elsewhere [16, 17]. In brief, OH^+ ions are generated by electron bombardment of low-pressure water vapour and are accelerated to form a beam with energy of 4.5 keV. The OH^+ ions are separated from the other main products of the ionisation, H_2O^+ and O^+, with a small electromagnet, and are then irradiated coaxially with output of a Coherent 699-29 c.w. single mode dye laser. Laser excitation of electronically excited OH^+ in its metastable $a^1\Delta$ and $b^1\Sigma^+$ states to levels of the predissociated $c^1\Pi$ state results in dissociation to form $O^+ + H$ or $O + H^+$ with yields dependent principally on the *e/f* rotational level symmetry, but also on J' and v'. For O^+ detection these fragment ions are separated from the parent OH^+ beam with a second electromagnet; neutral O atoms are detected directly along the laser irradiation axis. In both cases electron multipliers are used to record arrival of the O or O^+ products. Neutral fragment hydrogen atoms that would otherwise destroy this channel-selective detection method are not detected because the centre-of-mass kinetic energy release in the dissociation is sufficient for them to be ejected from the on-axis line-of-sight.

Acceleration of the beam to 4.5 keV results in a reduction in the velocity dispersion and so the Doppler width is typically ~90 MHz. Coupled with the use of a single–mode dye laser this enables high-precision wavelength measurement of lines in the optical region, observation of predissociation lifetime broadening, and, in some instances, resolution of nuclear hyperfine structure.

While the experimental technique enjoys high sensitivity, if a predissociation is slow compared with the ion flight time in the apparatus or so fast that a line is very strongly broadened then spectra may not be obtained. In some instances, such as the (0,0) vibrational band of the $c^1\Pi$ - $b^1\Sigma^+$ transition, the spectrum fell outside the available laser wavelength range. Theoretical predictions of the predissociation linewidth [13] indicate that this band should be readily observable in a fast-ion-beam experiment with an excited state lifetime in the ~10 ns range yielding narrow lines. It is also essential that the radiative decay times of the metastable states from which laser pumping occurs are long compared with the ion flight time to the irradiation region of a few microseconds. Calculations of $b^1\Sigma^+$ - $X^3\Sigma^-$ radiative lifetimes give values of ~1 ms for $v = 0$ and ~0.1 ms for $v = 1$ of the $b^1\Sigma^+$ state [18] which are long on the required timescale, and those for the $a^1\Delta$ state are expected to be much longer.

3. Spectroscopic Results

The photofragment spectrum of $^{16}OH^+$ with O^+ detection was recorded between 16 700 and 18 700 cm^{-1} and in selected regions down to 16 200 cm^{-1}. Over two hundred lines were observed, the vast majority of which have been assigned to the $c^1\Pi$ - $b^1\Sigma^+$ or $c^1\Pi$ - $a^1\Delta$ electronic transitions. The spectrum was also recorded in the O + H^+ channel but the frequency range was less comprehensive because the detection sensitivity is lower; in large part it was confined to a search for transitions already observed in the O^+ + H channel or predicted from analysis of these data. Of the approximately one hundred transitions recorded in the O + H^+ channel all bar one is assigned to one or other of the two singlet-singlet electronic transitions. Some transitions were detected in only one channel and some were seen in both channels, but in general excitation to $c^1\Pi$ rotational levels with *e* symmetry were observed through O atom detection and transitions to those with *f* symmetry were observed by recording O^+ ions. This results from a symmetry-selective dissociation, the general principles of which have been described [5]. Spectra of the $c^1\Pi$ - $b^1\Sigma^+$ system of $^{16}OD^+$ were also recorded in the range 16 800 – 17 500 cm^{-1} and have allowed confirmation of the vibrational numbering. The first spectra of the $c^1\Pi$ - $a^1\Delta$ electronic transition are reported here involving the v = 3 and 4 levels of the $a^1\Delta$ state and providing access to the v = 1 level of the $c^1\Pi$ state *via* the (1,3) band of this system. Approximate potential energy curves are given in Figure 1 and a summary of the bands recorded for $^{16}OH^+$ is given in Figure 2.

3.1 Transitions in the $c^1\Pi$ - $b^1\Sigma^+$ system

Rotational lines of the (2,0), (3,0), (4,1), (5,1) and (6,1) bands of $^{16}OH^+$ were recorded, as well as the (3,0), (4,0) and (5,1) bands of OD^+. Data for the (3,0) band of $^{16}OH^+$ were published earlier [4] but are included here in part for completeness and because some additional lines were measured. The measured wavenumbers are given in tables 1-9.

In $^{16}OH^+$ the (2,0) and (3,0) bands are the most intense and perturbations for $J' > 8$ are observed in all three rotational branches for both vibrational bands. This shows conclusively that the perturbations arise in the v = 0 level of the $b^1\Sigma^+$ state as inferred from complementary shifts in rotational line wavenumbers in the $A^3\Pi$ – $X^3\Sigma^-$ electronic transition due to $b^1\Sigma^+$ - $A^3\Pi$ interactions [1].

Three vibrational bands originating from the v = 1 level of the $b^1\Sigma^+$ state were observed but are weaker than those from v'' = 0 due to the lower population of v = 1 and less favourable Franck-Condon factors. Data from the (4,1), (5,1) and (6,1) bands are fragmentary comprising three P, six R and nine Q-branch lines for the (4,1) band, and only Q branches for the (5,1) and (6,1) bands with nine and five lines, respectively. The Q-branch lines of the (5,1) band are quite strong but despite extensive searching no P or R lines of this band were found. It is probable that the predissociation lifetimes of the v' = 5 *e* levels are so short that line-broadening reduces the sensitivity for detection of lines involving these levels. The (6,1) band origin lies to a wavelength shorter than is easily accessible with the dye laser but the Q branch is sufficiently red-degraded that the Q(9) to Q(13) lines could be observed. These Q-branch lines are of particular interest as

they are the only ones detected in the O^+ channel that show lifetime broadening; this is discussed further is section 4.3.5. No transitions from $v'' = 2$ or higher were observed even though they lie below the OH^+ dissociation limit. We presume that the combination of lower populations and smaller Franck-Condon factors rules out detection from these levels.

3.2 Transitions in the $c^1\Pi$ - $a^1\Delta$ system

Rotational lines of the (2,4), (3,4) and (1,3) bands were measured, the (2,4) band being the most extensively studied with five of the six possible branches observed. The (3,4) band resembles the (6,1) band of the c-b system in that its band origin lies to the blue of the easily accessible dye laser range but some lines in the three branches accessing the *f* components were recorded. In the case of the (1,3) band the three branches which access the upper *f* components have been measured and are found to be well behaved. Transitions to only three of the *e* rotational levels of the $v = 1$ $c^1\Pi$ state were observed and the lambda-doubling spacings in these levels are erratic with *e*-*f* level separations of +0.3723, -1.0147 and -7.4499 cm^{-1} for $J' = 4$, 5 and 6, respectively. The lowest rotational lines in the (1,3) and (2,4) bands exhibit a small splitting due to the nuclear spin (proton) – electron orbital hyperfine interaction.

3.3 Molecular parameters of the $a^1\Delta$, $b^1\Sigma^+$ and $c^1\Pi$ states

The rotational energy levels of the three electronic states were taken to be described by:

$$F(J, c^1\Pi) = B[J(J+1) - 1] - D[J(J+1) - 1]^2 + H[J(J+1) - 1]^3 \pm \tfrac{1}{2}[q + q_D J(J+1)]J(J+1)$$

$$F(J, b^1\Sigma^+) = BJ(J+1) - DJ^2(J+1)^2 + HJ^3(J+1)^3$$

$$F(J, a^1\Delta) = B[J(J+1) - 4] - D[J(J+1) - 4]^2 + H[J(J+1) - 4]^3 \pm \tfrac{1}{2} qJ(J+1)$$

where the ± sign refers to *e* and *f* levels, respectively, which correspond to parity $+(-1)^J$ and $-(-1)^J$ [19].

As the data cover a range of wavenumber precision (due to linewidth broadening and signal-to-noise considerations) and are limited to a few lines in some branches of some bands, we elected to fit simultaneously those bands which shared common levels. Broadly this also matched this 'quality' criterion. The (2,0) and (3,0) bands of the $c^1\Pi$ - $b^1\Sigma^+$ system of $^{16}OH^+$ together with the (2,4) and (3,4) bands of the $c^1\Pi$ - $a^1\Delta$ system were fitted using a least-squares routine to yield the molecular constants in table 10. Those lines involving perturbed rotational levels of the $b^1\Sigma^+$ state were omitted from this fit but were incorporated explicitly in a global fit of singlet and triplet data as described in section 3.4.

The three bands of the $c^1\Pi$ - $b^1\Sigma^+$ system of $^{16}OH^+$ involving $v'' = 1$ were fitted together but as relatively few lines were observed the resulting parameters in table 10 are less well determined than for other vibrational levels in the table. Lambda-doubling parameters could not be obtained for $v = 5$ and 6 of the $c^1\Pi$ state owing to the absence

of transitions to *e*-type levels. The (1,3) vibrational band of the $c^1\Pi$ - $a^1\Delta$ system was fitted but the information is limited to rotational parameters as almost all observed transitions involve the *f* components of the excited state levels.

For OD^+ lines of the (3,0) band were measured and fitted. The parameters from the (3,0) band analysis are given in table 6; the $v = 0$ level is found to exhibit perturbations as expected from the $A^3\Pi$ - $X^3\Sigma^-$ electronic band system of OD^+ observed in emission and only those lines with $J' < 8$ were included in the fit. Just two R-lines of the (4,0) band were available due to laser coverage, and only Q-lines were found for the 5-1 band despite an extensive search.

3.4 Singlet-triplet ($A^3\Pi$-$b^1\Sigma^+$) perturbation

Perturbations are observed in the $b^1\Sigma^+$ $v = 0$ level as a result of the interactions with the $v = 1$ level of the $A^3\Pi$ state. We have fitted simultaneously the rotational line wavenumbers of the (1,0) $A^3\Pi$ - $X^3\Sigma^-$ emission band of Merer et al. [1] and the (3,0) $c^1\Pi$ - $b^1\Sigma^+$ absorption band. The procedure follows broadly that of [1], but the fitting of the lines is performed simultaneously (rather than the individual $X^3\Sigma^-$ and $A^3\Pi$ states with $b^1\Sigma^+$ interaction) and the explicit inclusion of the singlet-singlet transitions allows improved determination of the molecular parameters. The energy levels of the four electronic states involved were taken as follows:

$X^3\Sigma^-$ - the expressions of Miller & Townes [20] were used,

$A^3\Pi$ (*f* levels): These levels are not affected by the $b^1\Sigma^+$ state. The Hamiltonian used is given in [1].

$A^3\Pi$ (*e* levels)/$b^1\Sigma^+$: The interaction between the $b^1\Sigma^+$ and $A^3\Pi$ states is accounted for by the addition of an off-diagonal spin-orbit matrix element

$$\left\langle {}^3\Pi_{0e} \middle| H \middle| {}^1\Sigma^+ \right\rangle = H_{so} R_{10}$$

where H_{so} is the spin-orbit interaction constant and R_{10} is the Franck-Condon factor [1].

$c^1\Pi$ and $b^1\Sigma^+$: These levels are represented by the equations in section 3.3.

Using these Hamiltonians, 37 $c^1\Pi$ - $b^1\Sigma^+$ and 361 $A^3\Pi$ - $X^3\Sigma^-$ rotational lines were fitted using 25 parameters. A few isolated lines of the triplet system that were not expected to be perturbed were found to fit poorly and were excluded from the final fit. The resulting parameters are given in table 11. The $A^3\Pi$ parameters are determined to a greater precision than previously and the value for the spin-orbit interaction parameter $H_{so}R_{10}$ in particular is improved. An attempt was made to allow for a rotational dependence of $H_{so}R_{10}$, but no improvement in the fit was achieved. The *T* values for the $A^3\Pi$ state differ from those of [1] by a constant value of 4.41(16) cm^{-1}, the origin of which we have not been able to determine.

4. Dissociation dynamics of OH^+ $c^1\Pi$ (v = 1-6)

In this section we describe dissociation from $c^1\Pi$ levels to form $O^+ + H$ and $O + H^+$, the partitioning between these dissociation channels and the mechanisms that govern the predissociation.

4.1 Electronic states and dissociation of OH^+

The main electronic states involved in the predissociation of the $c^1\Pi$ state are illustrated in Figure 1. The $c^1\Pi$ levels accessed in the experiments described here lie well above the first two OH^+ dissociation limits, $O^+(^4S) + H(^2S)$ and $O(^3P) + H^+$, which, because of the very similar first ionisation energies of O and H atoms, are almost degenerate. Figure 1 shows that the $c^1\Pi$ state is crossed by repulsive $^5\Sigma^-$ and $^3\Sigma^-$ curves, that the $c^1\Pi$ levels lie in the dissociation continua of the $X^3\Sigma^-$ and $A^3\Pi$ states, and that $c^1\Pi(e)$ levels can interact with those of the nearby $b^1\Sigma^+$ state. From $v' = 2$ data it was deduced [5] that for low values of v, both e and f levels could predissociate by coupling to the $^5\Sigma^-$ state which correlates with $O^+ + H$. However, for e levels, an additional indirect mechanism operates in which they interact with predissociated levels of the $b^1\Sigma^+$ state through rotational-electronic coupling. The $b^1\Sigma^+$ levels are strongly predissociated, with lifetimes of a few ps [18], due to spin-orbit coupling with the fully dissociative part of the $A^3\Pi$ state which correlates to $O + H^+$.

It was found for $v = 2$ that low-J e-type levels decay competitively to form both $O^+ + H$ and $O + H^+$ with higher-J e-levels decaying to form $O + H^+$. However, f levels of all observed J values dissociate exclusively to form $O^+ + H$ [5]. Transitions to the f-levels exhibit the same (Doppler-limited) linewidth of ~90 MHz indicating relatively long predissociation lifetimes, but the experimental e-level linewidths increase linearly with $J(J+1)$. This behaviour was rationalised in terms of a rotational-electronic interaction between $c^1\Pi(e)$ rotational levels and the $b^1\Sigma^+$ state which itself is coupled to the continuum of the $A^3\Pi$ state by a spin-orbit interaction and correlates with $O + H^+$. As this mechanism is open only to e-levels of the $c^1\Pi$ state, the f-levels are unaffected and decay principally *via* a repulsive $^5\Sigma^-$ state which correlates to $O^+ + H$. A calculation of the J-dependent predissociation lifetimes for the e-levels of $v' = 2$ assuming the $c^1\Pi(e) \sim b^1\Sigma^+ \sim A^3\Pi$ mechanism resulted in good overall agreement between observed and calculated widths; for example the $J'(e) = 1$ width was 7.3 MHz (folded within the ~100 MHz Doppler width) and the $J' = 9$ width 330 MHz compared with 260 (20) MHz measured in the experiment. Noting that for a $c^1\Pi - b^1\Sigma^+$ transition the P and R lines in absorption access e-levels and the Q lines access f-levels, some of the characteristics of this behaviour in the (3,0) band are illustrated in Figure 3. The Q(3) line appears strongly in the O^+ channel but is absent from the O channel, whereas the R(5) line is weak for O^+ detection but strong in the $O + H^+$ channel. The R(5) line is also noticeably broader than the Q(3) line.

4.2 Competition between dissociation channels (e-levels)

The (2,0) and (3,0) bands provide the most comprehensive set of data on the competition between the $O^+ + H$ and $O + H^+$ dissociation channels. The normalised measured rotational line intensities are shown in Figures 4-7. The pattern of branch intensity behaviour is similar for the two bands but the P and R branches are clearly

weaker relative to the Q branch for $v' = 2$ (Figure 6) than for $v' = 3$ (Figure 4). This means that *e*-levels have a greater propensity to decay to form $O + H^+$ from $v = 2$ than $v = 3$, with a ratio of O/O^+ for $v' = 3$ for $J' = 1$ quite close to unity. As the lambda-doubling parameter for $v' = 3$ is larger than that for $v' = 2$ (0.0835 *c.f.* 0.0616 cm^{-1}) and the $v' = 3$ lines for moderate to high values of J' are broader than for $v' = 2$, the opposite result might have been expected. However, the O/O^+ branching ratio is determined by *competition* between decay channels and dissociation of both *e* and *f* levels of $v' = 3$ *via* the $^5\Sigma^-$ state to form $O^+ + H$ is more favoured for $v' = 3$ than $v' = 2$. This arises as $v' = 3$ is nearer to the crossing of the $^5\Sigma^-$ state with the $c^1\Pi$ state.

Figure 8 shows the line intensities measured for the rotational lines of OD^+ in the O^+ channel where it is seen that the P and R lines are relatively much stronger with respect to the Q branch in comparison with $v = 2$ and 3 of $^{16}OH^+$. This can be rationalised as a weaker rotational-electronic interaction resulting in a lower propensity for the $v = 3$ *e* levels of OD^+ to decay to the $O + H^+$ fragments.

Although the O^+ and O atom fluxes could be measured simultaneously, a direct measurement of the branching ratio cannot be made because the collection efficiency and signal amplification for the two channels is unknown. However, an estimate of the branching ratio was made as follows. The Q-branch intensities were used to calculate the populations of the $v = 0$ $b^1\Sigma^+$ rotational levels. These were then used to predict the expected R and P line intensities which were then compared with those detected in the O^+ channel (where they are weak due to competition with O atom production). The results are shown in Figure 9.

4.3 Dissociation mechanisms and linewidths: experiment and theory

We describe here the linewidth results alongside the branching behaviour described, and make quantitative comparison between the observations and calculations. We first consider two theoretical approaches to the problem.

Using a combination of experimental and theoretical information, the linewidths of the $v = 2$ *e*-levels were calculated as follows [21]. The linewidth Γ of a $c^1\Pi(e)$ level *v, J* is given by:

$$\Gamma_{v(\Pi,e)} = \Gamma_{v(\Sigma)} \left[\left\langle {}^1\Pi \left| L_+ \right| {}^1\Sigma^+ \right\rangle \right]^2 J(J+1) \left[\sum_{v(\Sigma)} \frac{B_{v(\Pi),v(\Sigma)}}{\left| \Delta E_{v(\Pi),v(\Sigma)} \right|} \right]^2$$

where $\Gamma_{v(\Sigma)}$ is the predissociation linewidth for vibrational level *v* of the $b^1\Sigma^+$ state due to spin-orbit interaction with the $A^3\Pi$ state (known from calculation to be 2-3 ps for the relevant levels [18]), $\Delta E_{v(\Pi),v(\Sigma)}$ is the vibrational energy level separation, and

$$\left\langle {}^1\Pi \left| L_+ \right| {}^1\Sigma^+ \right\rangle$$

is the matrix element of the rotational-electronic operator with numerical value from the experimental lambda-doubling parameter, *q*. The values for $B_{v(\Pi),v(\Sigma)}$, defined through

$$B_{v(\Pi),v(\Sigma)} = \left\langle v(\Pi)\left| h^2/8\pi^2\ \mu R^2 \right| v(\Sigma)\right\rangle,$$

were calculated by numerical integration using wavefunctions derived from RKR $c^1\Pi$ and *ab-initio* $b^1\Sigma^+$ potential curves [5]. The results for v = 2 were interpreted successfully as this reproduces the linear dependence of the linewidth on $J(J+1)$ and the quantitative width as noted in section 4.1.

In an important study, Yarkony has approached the predissociation problem from a fully *ab-initio* viewpoint based on electronic structure calculations of the potential energy curves and couplings between states [13]. The possible couplings are discussed in his paper in great detail and can be summarized as:

(a) $c^1\Pi \sim {}^5\Sigma^-$ (dipolar spin-spin and 2nd order spin-orbit) ($O^+ + H$),
(b) $c^1\Pi \sim {}^3\Sigma^-$ (spin-orbit interaction) ($O^+ + H$),
(c) $c^1\Pi \sim A^3\Pi$ (spin-orbit interaction) ($O + H^+$),
(d) $c^1\Pi \sim b^1\Sigma^+ \sim A^3\Pi$ (rotational electronic, spin orbit) ($O + H^+$),
(e) $c^1\Pi \sim a^1\Delta \sim A^3\Pi$ (rotational electronic, spin orbit) ($O + H^+$),

where the interactions are first order unless stated otherwise and the fragmentation products are given in parentheses. Key results of the study are that for levels v = 0-3, on which the work was focussed, the mechanisms (a) and (d) are dominant, but that for higher v (b) also becomes significant. It is of interest to compare these *ab-initio* results with experimental results and we now consider each of the $c^1\Pi$ levels with v' = 1-6 in turn.

4.3.1 v' = 1

Levels of v' = 1 were explored experimentally *via* the relatively weak (1,3) band of the $c^1\Pi$ - $a^1\Delta$ system. The *f* levels undergo predissociation with Doppler-limited linewidths and are well behaved, but the three transitions found involving *e* levels (J' = 4, 5 and 6) have rapidly varying linewidths of 500, 900 and 2000 MHz, the increase being in the same sense as the change in lambda-doublet splitting for these J levels (see 3.2). This behaviour can be traced to the near-degeneracy of v' = 1 ($c^1\Pi$) with v = 6 of the $b^1\Sigma^+$ state. In general the *e* linewidths for v = 1 are predicted [13] to be higher than for v = 2 and 3, and it was noted [13] that small shifts in the relative energies of the potential energy curves introduced major changes in the widths. The v = 1 level is 'anomalous' in the sense that it exhibits an extreme sensitivity to the relative state energies and a quantitative calculation that reproduces the experimental results remains to be performed.

4.3.2 v' = 2 and 3

Results for v' = 2 have been described [5] and are summarized in section 4.1. The linewidths and the J-dependence for *e*-levels can be accounted for well by both the published analysis [5] and *ab-initio* calculations [13]. Both theoretical approaches predict a linewidth increase that is essentially linear in $J(J+1)$, though the *ab-initio* results suggest a slight curvature for v = 3 [13]. In order to make the best possible comparison we have convolved the theoretical (Lorentzian) data for the $c^1\Pi \sim b^1\Sigma^+ \sim A^3\Pi$ contribution [13] with a Gaussian function for the laboratory (Doppler) width to

generate a Voigt profile. The measured experimental and theoretically adjusted (Voigt profile) results are shown in Figure 10 and show a remarkable level of agreement. Factors that could play a role in generating the slight differences include power-broadening in the laboratory spectra, neglect in this treatment of the linewidth contribution from predissociation *via* the $^5\Sigma^-$ state which is predicted to contribute *c.* 40 MHz and 10 MHz for v = 2 and 3 respectively [13], possible quantum interference effects, and slight uncertainty in the relative state term values which might be the origin of the curvature in the theoretical v = 3 data.

Combining the experimental partitioning data (Figure 9) and the linewidth measurements with the results of both perturbation and *ab-initio*-based theory [13] allows quite a detailed description of the dissociation as a function of J. This is illustrated in the results of Yarkony (fig 7 of [13]) where it is seen that for v' = 3 and J' up to ~3 the interaction of *f (*and *e)* levels with $^5\Sigma^-$ (Ω =1) to form $O^+ + H$ is a significant and almost J-independent predissociation mechanism with Γ ~ 40 MHz; the strongly $J(J+1)$-dependent $c^1\Pi$(e) ~ $b^1\Sigma^+$ ~ $A^3\Pi$ mechanism is less significant up to J' ~ 3 but takes over rapidly for *e* levels with moderate to high J-values to give $O + H^+$.

4.3.3 v' = 4

The data for v' = 4 is less comprehensive with only eighteen P, Q and R lines available from the (4,1) band. For v' = 4 *e*-levels, the experimentally measured linewidth increases from 200 to 400 MHz from J' = 2 to 5. Hence the predissociation is stronger than for v = 3 which is itself stronger than for v = 2. The result for v = 4 is not unexpected as the measured lambda-doubling parameter $q(^1\Pi)$ increases as 0.062, 0.083 and 0.145 cm^{-1} for v = 2, 3 and 4, respectively.

4.3.4 v′ = 5

For these two vibrational levels only Q branches that involve *f* levels were observed. For v = 5 the Q-branch lines are readily detected and have Doppler-limited linewidths, but an extensive search for transitions to the *e* components proved fruitless. A likely explanation is that the levels are very strongly broadened by interaction between v = 5 ($c^1\Pi$) and v = 9 ($b^1\Sigma^+$) for which a very large lambda-doubling q value of –0.36 cm^{-1} for the $c^1\Pi$ is estimated using a calculated value of $B_{v(\Pi),v(\Sigma)}$ as discussed in section 4.3.

4.3.5 v' = 6

In the case of v = 6 only Q(9) to Q(13) lines were observed due to a restricted laser coverage but exhibit measurable lifetime broadening with a weak dependence on rotational quantum number. The measured linewidths for v' = 6, J' = 9, 10, 11, 12 and 13 are 385, 410, 425, 525 and 625 MHz, respectively. It is probable that this predissociation is dominated by the curve crossing with the repulsive $^3\Sigma^-$ state but this has yet to be addressed theoretically. The strongest predicted R and P lines fall outside the range of laser coverage.

5. Summary and conclusion

We have conducted a combined spectroscopic and dynamical study of photodissociation spectra ($c^1\Pi$ - $b^1\Sigma^+$ and $c^1\Pi$ - $a^1\Delta$) of the OH^+ molecule and the predissociation of its $c^1\Pi$ state. Spectroscopic parameters are reported for ten vibrational levels of $^{16}OH^+$ and two of OD^+. Perturbations in $v = 0$ of the $b^1\Sigma^+$ state due to $v = 1$ of $A^3\Pi$ are observed in the $c^1\Pi$ - $b^1\Sigma^+$ system and combined with transitions of the $A^3\Pi$ – $X^3\Sigma^-$ system observed in emission [1] to yield parameters for the four electronic states. The $c^1\Pi$ state is observed to predissociate from v = 1-6 and shows a remarkable selectivity in its dissociation to form $O^+ + H$ and/or $O + H^+$ according to the *e/f* symmetry of the rotational level. We find good agreement between experiment and theory for the *e*–level predissociation rates.

Acknowledgements

Peter Sarre thanks John Brown most warmly for his encouragement, inspiration and spectroscopic insight over many years. We thank the Engineering and Physical Sciences Research Council and The University of Nottingham for research grants and financial support, and Jane Burrows for assistance in the preparation of this paper.

References

[1] A.J. Merer, D.N. Malm, R.W. Martin, M. Horani, J. Rostas, *Can. J. Phys.*, **53**, 251 (1975)

[2] H. Helm, P.C. Cosby, D.L. Huestis, *Phys. Rev.A*, 30, 851 (1984)

[3] J. Levin, U. Hechtfischer, L. Knoll, M. Lange, G. Saathoff, R. Wester, A. Wolf, D. Schwalm, D. Zajfman, *Hyperfine Interactions,* **127**, 267 (2000)

[4] D.J. Rodgers, P.J. Sarre, *Chem. Phys. Lett.* **143,** 235 (1988)

[5] A.P. Levick, T.E. Masters, D.J. Rodgers, P.J. Sarre, Q.-S. Zhu , *Phys. Rev. Lett.,* **63**, 2216 (1989)

[6] M.H.W. Gruebele, R.P. Muller, R.J. Saykally, *J. chem. Phys.,* **84**, 2489 (1986)

[7] J.P. Bekooy, P. Verhoeve, W.L. Meerts, A. Dymanus, *J. chem. Phys.,* **82**, 3868 (1985)

[8] P. Verhoeve, J. P. Bekooy, W. L. Meerts, J. J. ter Meulen, A. Dymanus, *Chem. Phys. Lett.*, **125**, 3286 (1986)

[9] M.W. Crofton, R.S. Altman, M.F. Jagod, T. Oka, *J. phys. Chem.* **89**, 3614 (1985)

[10] B.D. Rehfuss, M.-F. Jagod, L.-W. Xu, T. Oka, *J. mol. Spectrosc.*, **151**, 59 (1992)

[11] D. Roth, S.A. Nizkorodov, J.P. Maier, O. Dopfer, *J. chem. Phys.*, **109**, 3841 (1998)

[12] T.D. Varberg, K.M. Evenson, J.M. Brown, *J. chem. Phys.,* **100**, 2487 (1994)

[13] D.R. Yarkony, *J. phys. Chem.* **97**, 111 (1993)

[14] J.T. Moseley, Adv. Chem. Phys. **60**, 245 (1985)

[15] S.G. Cox, A.D.J. Critchley, I.R. McNab, *Measurement Science & Technology*, **10**, 101 (1999)

[16] P.J. Sarre, J.M. Walmsley, C.J. Whitham, *Farad. Disc. Chem. Soc.*, **82**, 67 (1986)

[17] P.J. Sarre, J.M. Walmsley, C.J. Whitham, *Phil. Trans. Roy. Soc. Lond. A* **324**, 233 (1988)

[18] R. De Vivie, C.M. Marian, S.D., Peyerimhoff, *Chem. Phys.*, **112**, 349 (1987)

[19] J.M. Brown, J.T. Hougen, K.P. Huber, J.W.C. Johns, I. Kopp, H. Lefebvre-Brion, A.J. Merer, D.A. Ramsay, J. Rostas, R.N. Zare, *J. mol. Spectrosc.*, **55,** 500 (1975)

[20] S.L. Miller, C.H. Townes, Phys. Rev., **90**, 537 (1953)

[21] H. Lefebvre-Brion, R.W. Field, *Perturbations in the Spectra of Diatomic Molecules,* Academic, London, 1986, p. 376.

Table 1
Vacuum wavenumbers of rotational lines (2,0) band of the $c^1\Pi$-$b^1\Sigma^+$ system of $^{16}OH^+$

J''	P(J'')	Q(J'')	R(J'')
0	-	-	17010.743
1	-	16978.028	17019.501
2	16913.021	16953.999	17016.283
3	16856.785	16917.943	17001.050
4	16788.800	16869.889	16973.772
5	16709.129	16809.835	16934.419
6	16617.829	16737.803	16882.976
7	16514.974	16653.810	16819.425
8	16400.632	16557.891	16743.778
9	-	16450.101	16656.068
10	-	16330.637	-
11	-	16200.480	-

Table 2
Vacuum wavenumbers of rotational lines of the (3,0) band of the $c^1\Pi$-$b^1\Sigma^+$ system of $^{16}OH^+$

J''	P(J'')	Q(J'')	R(J'')
0	-	-	18484.624
1	-	18451.869	18491.110
2	18386.905	18425.466	18484.488
3	18328.393	18385.878	18464.732
4	18257.003	18333.112	18431.821
5	18172.810	18267.184	18385.738
6	18075.878	18188.112	18326.494
7	17966.292	18095.935	18254.100
8	17844.158	17990.697	18168.590
9	17709.627	17872.479	18070.042
10	17562.954	17741.468	17958.671
11	-	17598.671	17835.497
12	-	17436.356	-
13	-	17269.952	-

Table 3
Vacuum wavenumbers of rotational lines of the (4,1) band of the $c^1\Pi$-$b^1\Sigma^+$ system of $^{16}OH^+$

J''	P(J'')	Q(J'')	R(J'')
0	-	-	16904.597
1	-	16873.380	16910.690
2	-	16848.016	16904.340
3	16756.236	16809.914	16885.465
4	16688.231	16758.998	16854.014
5	16607.885	16695.234	16809.951
6	-	16618.574	-
7	-	16529.012	-
8	-	16426.555	-
9	-	16311.236	-

Table 4
Vacuum wavenumbers of rotational lines of the (5,1) band of the $c^1\Pi$-$b^1\Sigma^+$ system of $^{16}OH^+$

J''	P(J'')	Q(J'')	R(J'')
1	-	18150.959	-
2	-	18123.330	-
3	-	18081.827	-
4	-	18026.395	-
5	-	17956.978	-
6	-	17873.548	-
7	-	17776.092	-
8	-	17664.624	-
9	-	17539.179	-

Table 5
Vacuum wavenumbers of rotational lines of the (6,1) band of the $c^1\Pi$-$b^1\Sigma^+$ system of $^{16}OH^+$

J''	P(J'')	Q(J'')	R(J'')
9	-	18668.157	-
10	-	18517.436	-
11	-	18351.706	-
12	-	18171.049	-
13	-	17975.600	-

Table 6
Vacuum wavenumbers of rotational lines of the (3,0) band of the $c^1\Pi$-$b^1\Sigma^+$ system of $^{16}OD^+$

J''	P(J'')	Q(J'')	R(J'')
0	-	-	17497.545
1	-	17480.088	17501.948
2	17445.312	17467.007	17499.829
3	17414.943	17447.381	17491.184
4	17378.116	17421.229	17475.991
5	17334.865	17388.544	17454.263
6	17285.199	17349.342	17425.988
7	17229.150	17303.643	17391.180
8	17166.757	17251.466	17349.854
9	-	17192.851	17302.042
10	-	17127.886	-
11	-	17056.830	-
12	-	16981.444	-

Table 7: Vacuum wavenumbers of rotational lines of the (2,4) band of the $c^1\Pi$-$b^1\Delta$ system of $^{16}OH^+$

J''	P(J'')	Q(J'')	R(J'')
2e	17570.105	17611.450	-
2f	17569.999	17611.966	-
3e	17528.959	17590.875	-
3f	17528.605	17590.141	17671.983
4e	17481.074	17563.426	-
4f	17480.338	17562.181	17664.153
5e	17426.480	17529.098	-
5f	17425.237	17527.207	17649.094
6e	17365.211	17487.882	-
6f	17363.319	17485.204	17626.740
7e	17297.290	17439.764	-
7f	17294.612	17436.151	17597.034
8e	17222.750	17384.730	-
8f	17219.132	17380.021	17559.908
9e	-	17322.770	-
9f	17136.901	17316.789	17515.299
10e	-	17253.865	-
10f	17047.923	17246.436	17463.140
11f	16952.211	17168.925	17403.366
12f	16849.774	17084.223	17335.902
13f	16740.608	16992.295	17260.680
14f	16624.717	16893.114	17177.630
15f	16502.092	16786.633	17086.684
16f	-	16672.819	-
17f	-	16551.637	-

Table 8
Vacuum wavenumbers of rotational lines of the (3,4) band of the $c^1\Pi$-$b^1\Delta$ system of $^{16}OH^+$ (*f* upper levels)

J″	P(*J″*)	Q(*J″*)	R(*J″*)
7	18774.917	-	-
8	18661.252	-	-
9	18569.704	18739.154	-
10	18470.285	18657.247	-
11	18363.024	18567.087	-
12	18247.941	18468.662	18705.554
13	18125.051	18361.954	18614.498
14	-	18246.931	18514.576
15	-	18123.584	18405.748
16	-	17991.888	18287.949
17	-	17851.820	18161.124
18	-	17703.356	-
19	-	17546.474	-

Table 9
Vacuum wavenumbers of rotational lines of the (1,3) band of the $c^1\Pi$-$b^1\Delta$ system of $^{16}OH^+$ (*f* upper levels)*

J″	P(*J″*)	Q(*J″*)	R(*J″*)
2	18545.975	18589.539	-
3	18503.180	18568.402	18655.148
4	18453.451	18540.201	18648.284
5	18396.821	18504.928	18634.110
6	18333.313	18462.536	18612.557
7	18262.959	18413.009	18583.556
8	18185.755	18356.321	18547.037
9	18101.727	18292.450	18502.928
10	-	18221.352	18451.147
11	-	18142.986	18391.621
12	-	18057.333	18324.270
13	17697.395	17964.335	18249.011
14	17579.229	-	18165.769
15	17454.220	17756.098	-
16	17322.341	17640.774	-
17	17183.599	17517.909	-
18	17037.962	17387.465	17751.413
19	-	17249.396	17627.070
20	-	17103.656	17494.285

*Three lines (*e* upper components) of the (1,3) band were also measured, Q(4), Q(5) and Q(6) with wavenumbers of 18540.573, 18503.913 and 18455.087 cm^{-1}, respectively.

Table 10. Molecular parameters (in cm^{-1}) derived fitting as described in section 3.3. Values in parentheses are 3σ.

OH^+		$v = 0$	$v = 1$	$v = 2$	$v = 3$	$v = 4$	$v = 5$	$v = 6$
$c^1\Pi$	B_v		10.9093(3)[a]	10.3163(3)	9.7357(4)	9.192(4)	8.555(5)[a]	7.94(3)[a]
	D_v x 10^3		1.933(2)	1.813(3)	1.708(3)	1.64(10)	1.85(16)	1.14(22)
	H_v x 10^6		0.173(2)	0.151(5)	0.121(5)	3.2(7)	4.0(12)	
	q_v		-	0.0616(2)	0.0836(3)	0.145(2)		
	$q_{v,D}$ x 10^4		-	0.54(2)	1.13(4)	3.3(8)		
$b^1\Sigma^+$	B_v	16.2980(8)[b]	15.459(4)					
	D_v x 10^3	1.89(2)	0.88(11)					
	H_v x 10^6	-0.4(2)	-1.0(6)					
$a^1\Delta$	B_v				14.4288(4)	13.7724(3)		
	D_v x 10^3				1.753(2)	1.695(2)		
	H_v x 10^6				0.132(3)[c]	0.115(5)[c]		

OD^+					
$c^1\Pi$	B_v				5.4513(4)
	D_v x 10^3				0.53(1)
	H_v x 10^6				-0.3(2)
	q_v				0.0214(2)
	$q_{v,D}$ x 10^4				0.11(4)
$b^1\Sigma^+$	B_v	8.7150(5)[d]			
	D_v x 10^3	0.57(2)			
	H_v x 10^6	0.1(1)			

a. B value quoted is for f upper levels.
b. The corresponding values for B_0 ($b^1\Sigma^+$) from [1] is 16.320(15) cm^{-1}. Lines with $J' > 8$ were excluded.
c. Marginally determined values for $q_3 = 6(2) \times 10^{-5}$ cm^{-1} and $q_4 = 3(3) \times 10^{-5}$ cm^{-1} were obtained.
d. The value for B_0 ($b^1\Sigma^+$) from [1] is 8.7369(23) cm^{-1}. Lines with $J' > 8$ were excluded.
e. T values obtained (in cm^{-1}) are: c-b T_{02} = 17000.37(1), T_{03} = 18474.80(1), T_{41} = 16895.26(2), T_{51} = 18173.33(2), T_{61} = 19353.7(1.2), c-a T_{24} = 17614.80(1), T_{34}=14744.42(1).

Table 11.

Molecular parameters (in cm^{-1}) from least-squares fitting of the (1,0) $A^3\Pi$ - $X^3\Sigma^-$ emission band of Merer et al. [1] and the (3,0) $c^1\Pi$ - $b^1\Sigma^+$ band measured in this work.

		Merer et al.[1]*	This work
$X^3\Sigma^-$ $v = 0$	B	16.42233(77)	16.42319(161)
	D x 10^3	1.91744(242)	1.92140(656)
	H x 10^6	0.12394(210)	0.12835(782)
	λ	2.1344(115)	2.1424(216)
	γ	-0.1478(14)	-0.1485(23)
$A^3\Pi$ $v = 1$	T_{0+}	30002.05(11)	30006.47(5)
	T_{0-}	30008.24(11)	30012.63(6)
	T_1	29922.98(11)	29927.40(5)
	T_2	29839.34(10)	29843.81(15)
	B	12.4973(11)	12.4981(15)
	D x 10^3	2.183(5)	2.189(6)
	H x 10^6	0.083(8)	0.088(7)
	p	-0.2354(112)	-0.2376(50)
	q	0.0440(16)	0.0443(7)
	A_D	0.0052(10)	0.0041(6)
	q_D x 10^5	-2.32(40)	-2.19(19)
	$H_{so}R_{10}$	75.86(101)	76.99(2)
$b^1\Sigma^+$ $v = 0$	T_0	29058.76(221)	29063.23(119)
	B	16.320(15)	16.307(8)
	D x 10^3	1.92(fixed)	1.89(20)
$c^1\Pi$ $v = 3$	T_3	-	18473.20(7)
	B	-	9.736(8)
	D x 10^3	-	1.70(6)
	q	-	0.084(6)
	q_D x 10^4	-	1.1(9)

* Parameters for $X^3\Sigma^-$ $v = 0$ measured by infrared, LMR and sub-mm spectroscopy [6-10] are compared in [10].

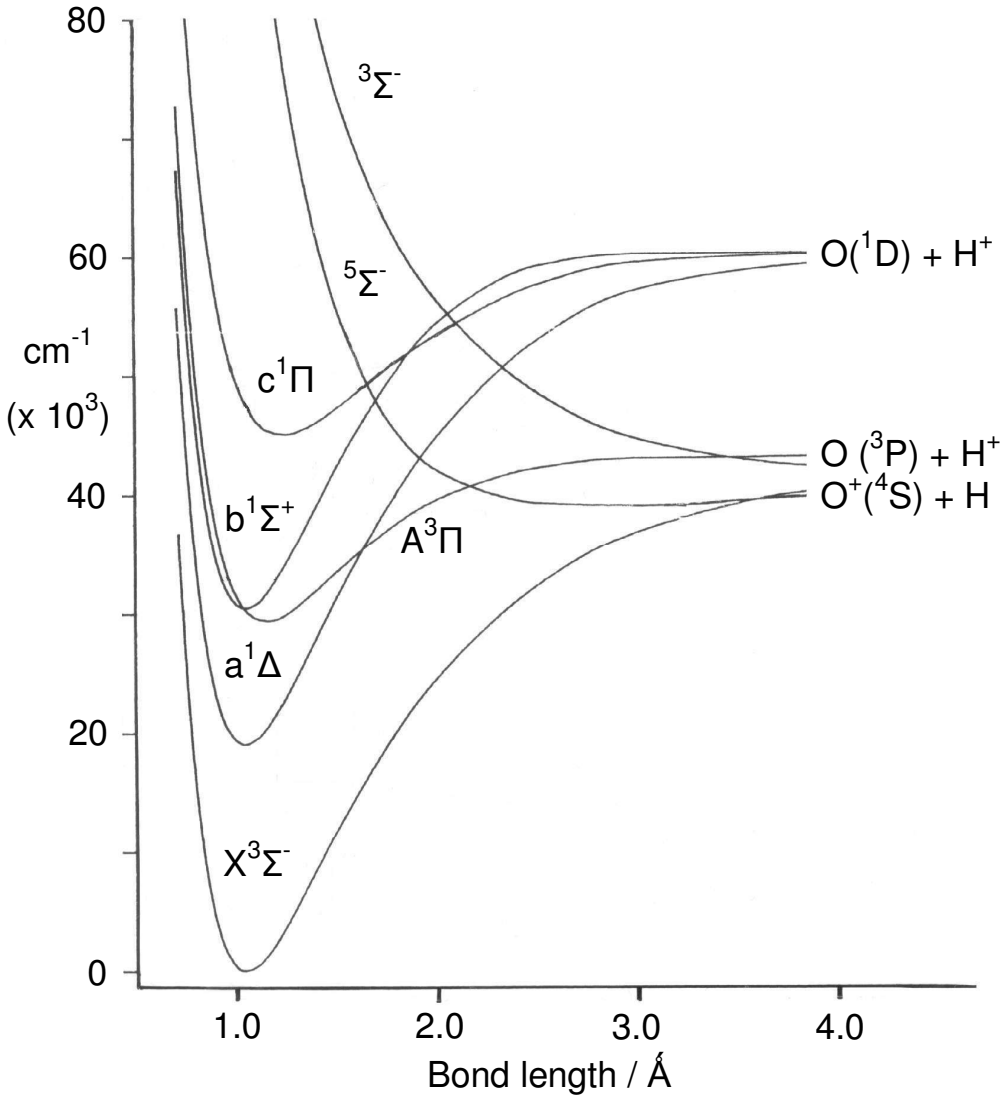

Figure 1. Potential energy curves of the seven electronic states of OH^+ that are involved in this study, as described in [5]. The two lowest dissociation asymptotes are (in reality) almost degenerate at high internuclear separation.

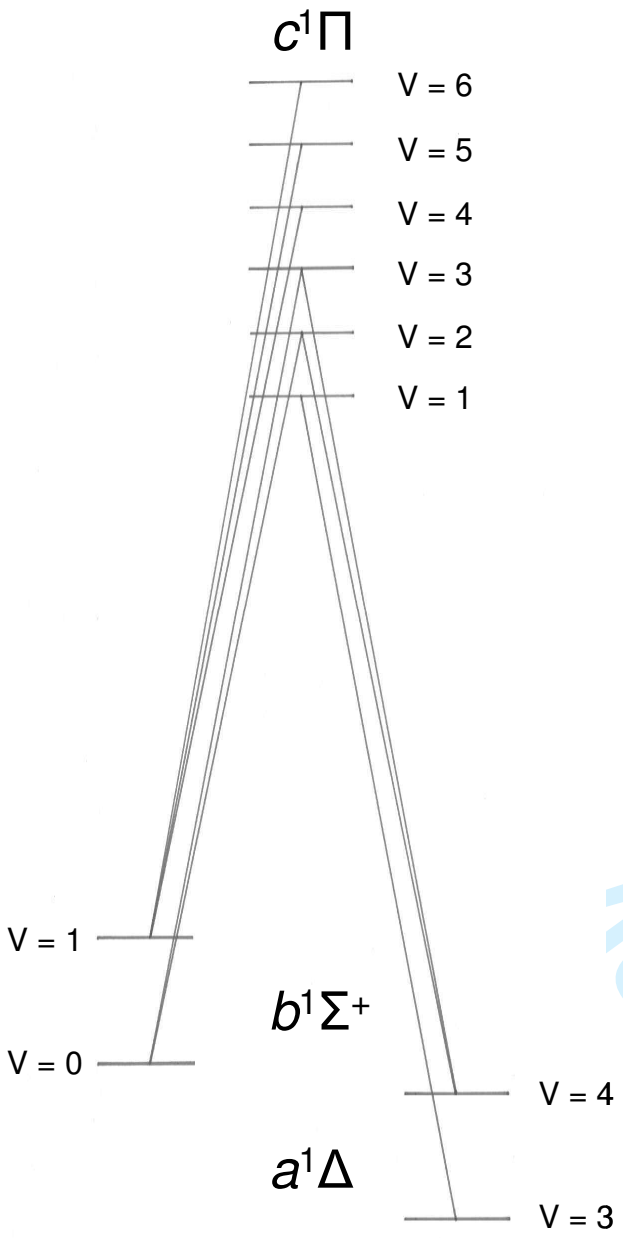

Figure 2. Schematic representation of the bands of $^{16}OH^+$ observed.

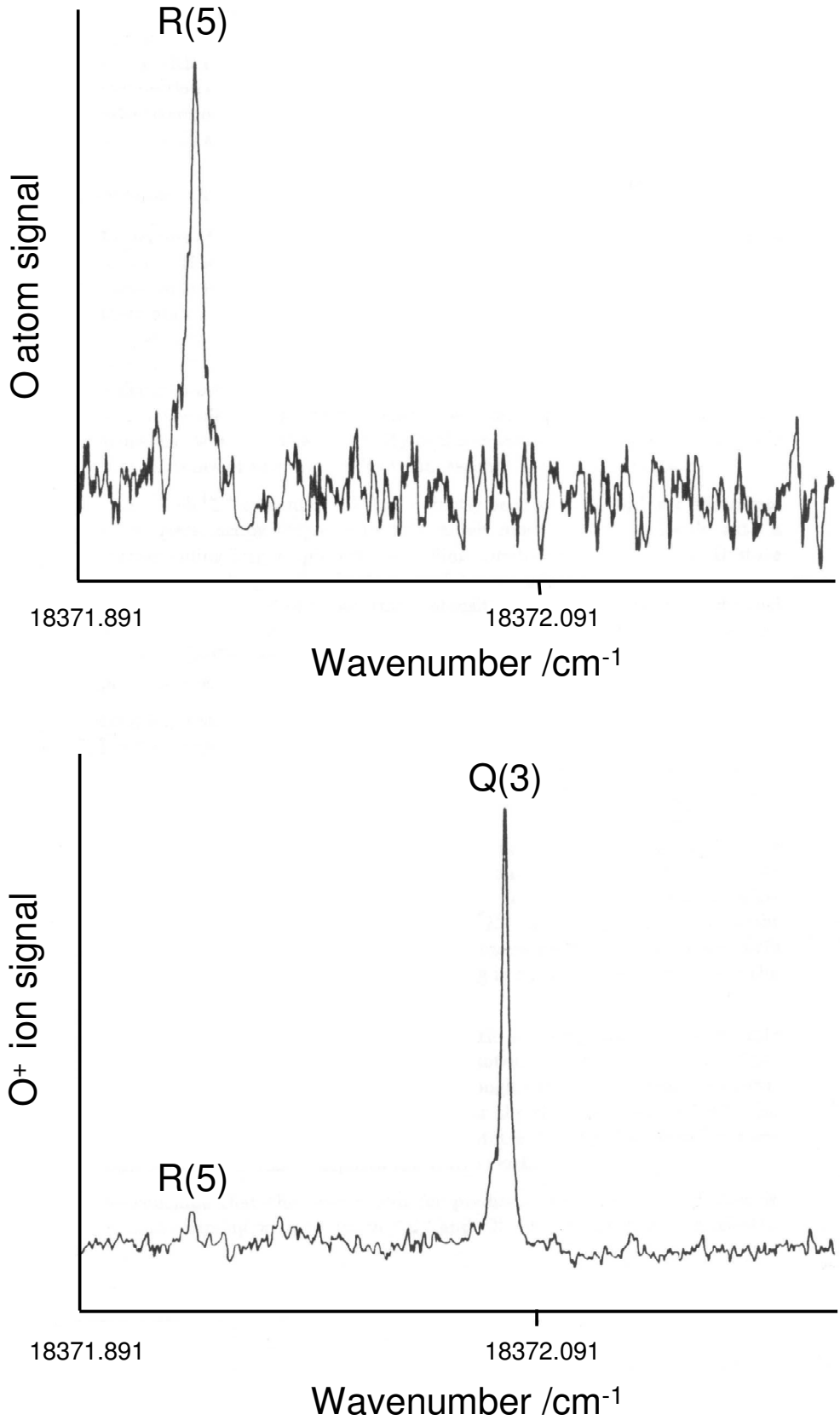

Figure 3. Spectra recorded in the O^+ ion and O atom channels showing competitive dissociation for excitation in the R(5) line to the $v' = 3$, $J' = 6(e)$ level. The wavenumbers are as recorded in the laboratory and are not corrected for the experimental Doppler shift.

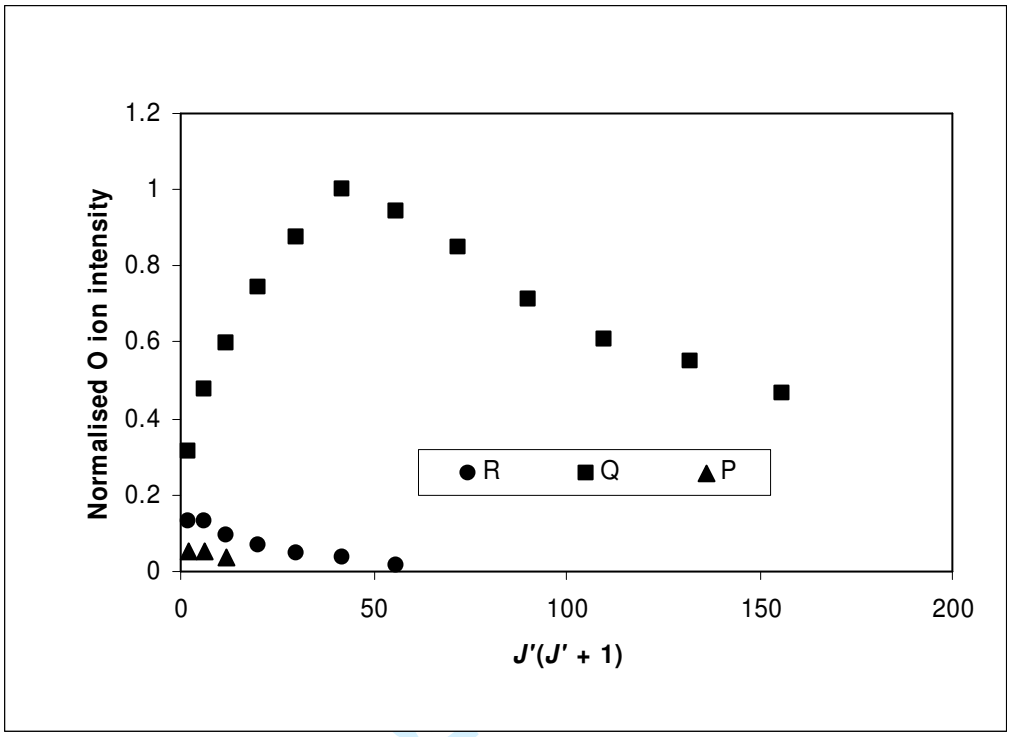

Figure 4. Normalised intensities of the P, Q and R lines of the (3,0) band of the $c^1\Pi$-$b^1\Sigma^+$ system of $^{16}OH^+$ recorded in the O^+ ion channel.

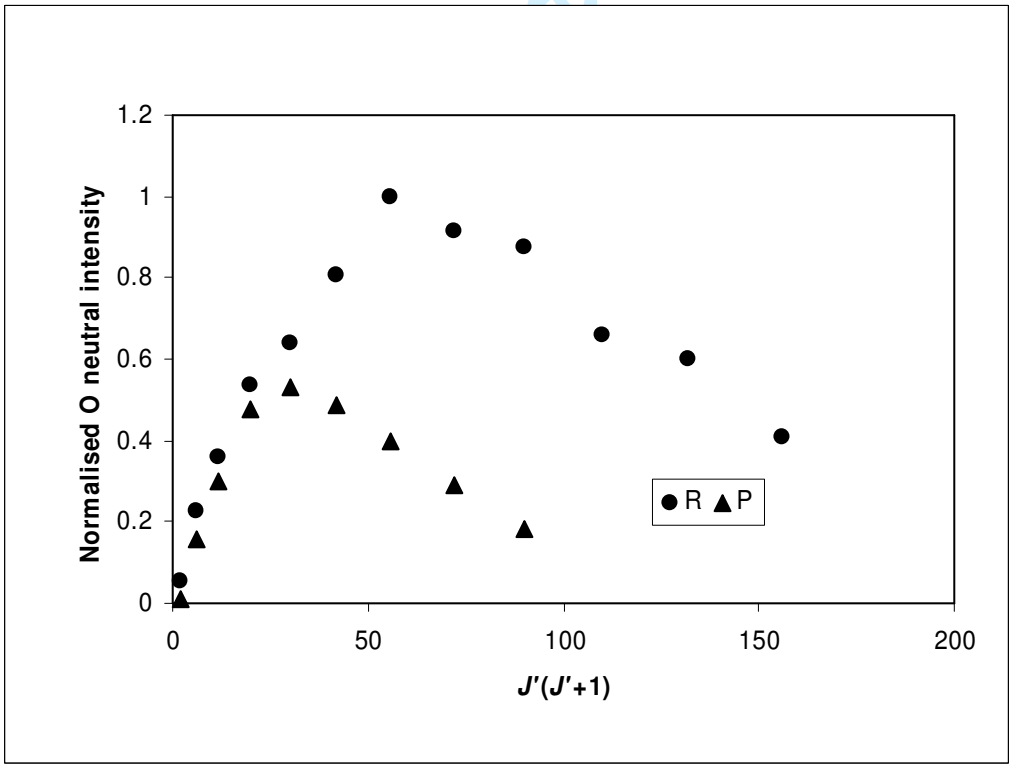

Figure 5. Normalised intensities of the P and R lines of the (3,0) band of the $c^1\Pi$-$b^1\Sigma^+$ system of $^{16}OH^+$ recorded in the O atom channel.

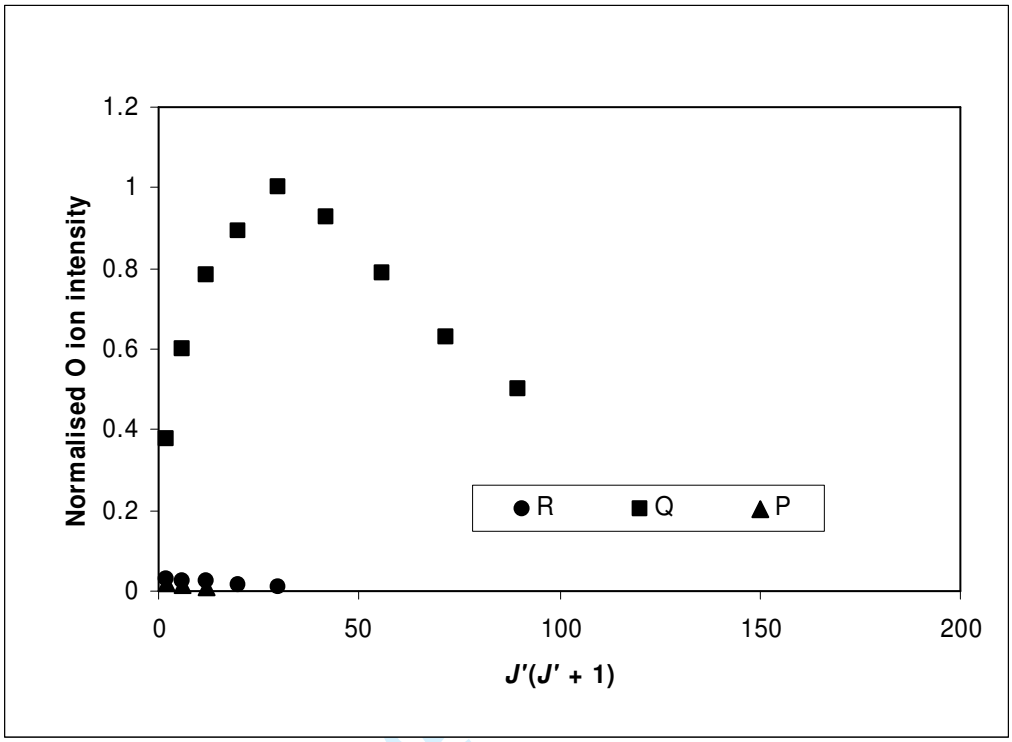

Figure 6. Normalised intensities of the P, Q and R lines of the (2,0) band of the $c^1\Pi$-$b^1\Sigma^+$ system of $^{16}OH^+$ recorded in the O^+ ion channel.

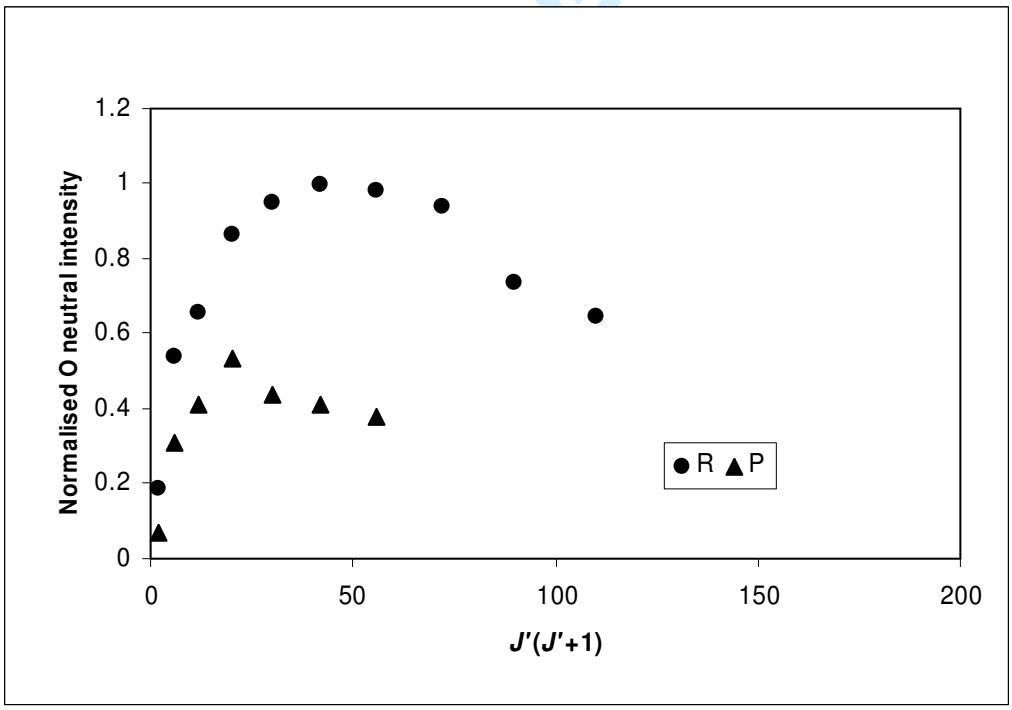

Figure 7. Normalised intensities of the P and R lines of the (2,0) band of the $c^1\Pi$-$b^1\Sigma^+$ system of $^{16}OH^+$ recorded in the O atom channel.

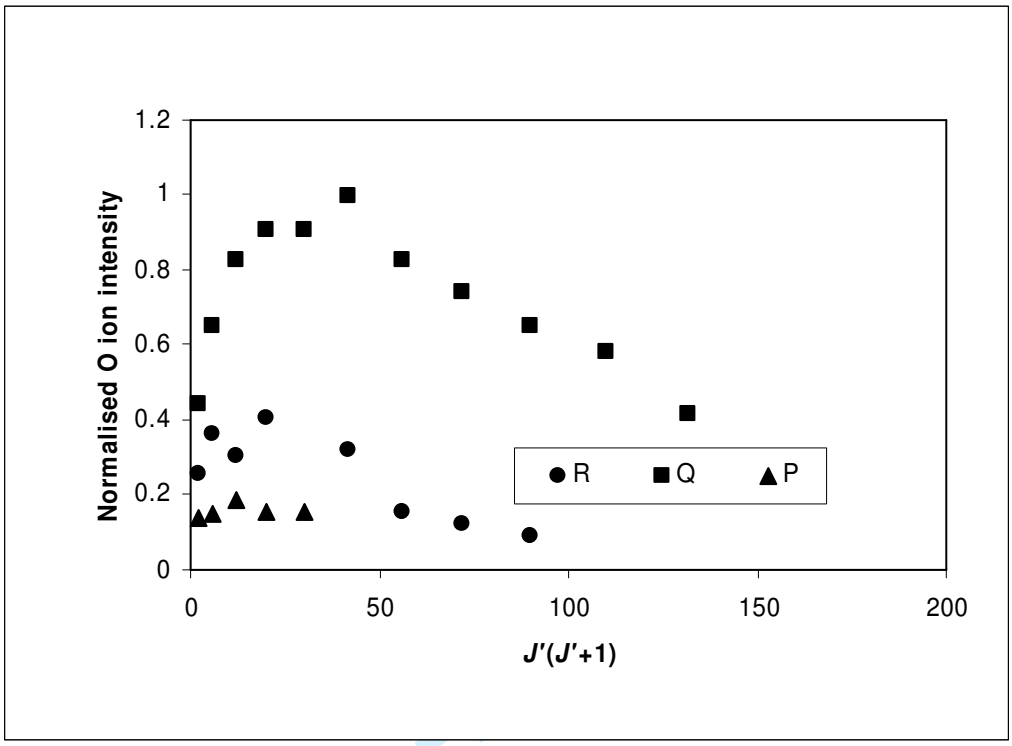

Figure 8. Normalised intensities of the P, Q and R lines of the (3,0) band of the $c^1\Pi$-$b^1\Sigma^+$ system of $^{16}OD^+$ recorded in the O^+ ion channel.

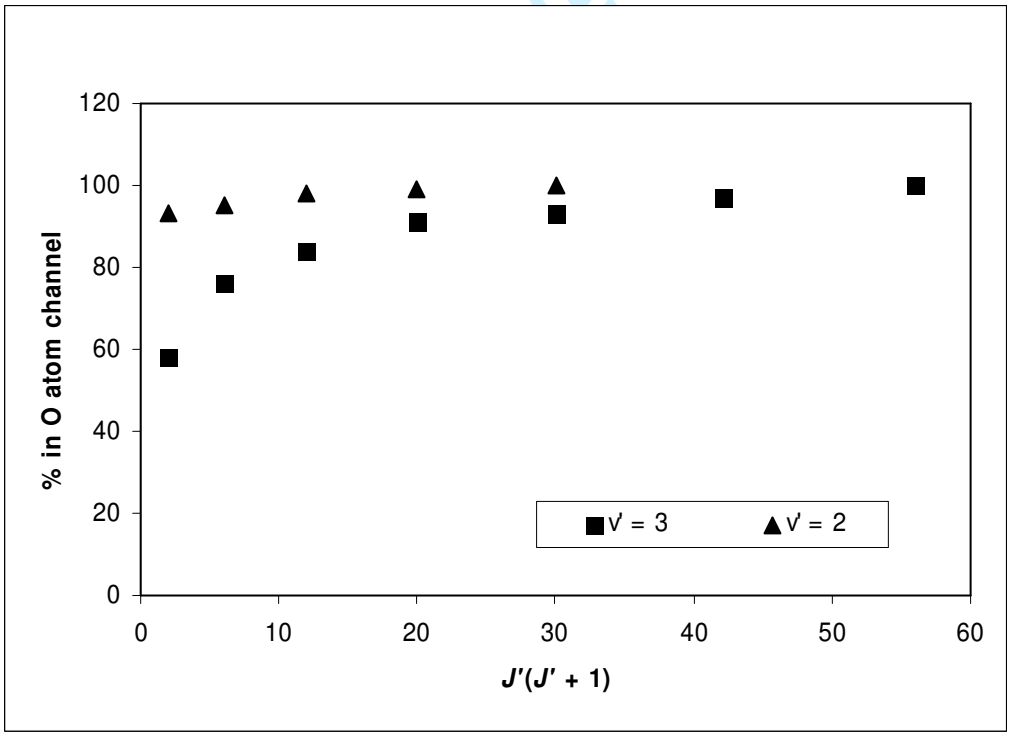

Figure 9: Branching into the $O + H^+$ channel from *e*-levels of $v' = 2$ and 3 of the $c^1\Pi$ as deduced from line intensity measurements.

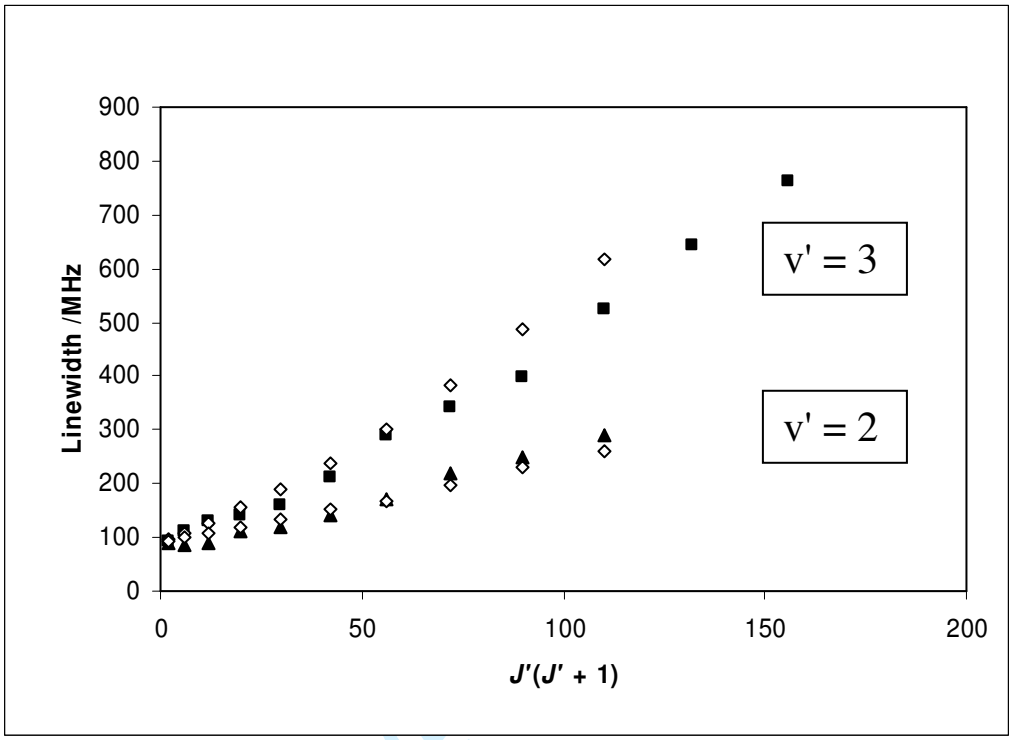

Figure 10: Linewidths for $v' = 3$ (squares) and $v' = 2$ (triangles) and the corresponding theoretical results (open diamonds) [13] for the decay of *e*-levels. The experimentally measured linewidths were adjusted for the effect of the laboratory Doppler width as described in section 4.3.2.